IEEE Access
Multidisciplinary ⋮ Rapid Review ⋮ Open Access Journal

Received November 8, 2020, accepted November 27, 2020, date of publication December 4, 2020,
date of current version December 17, 2020.

Digital Object Identifier 10.1109/ACCESS.2020.3042557

Incipient Fault Location Method of Cable Based on Both-End Electric Quantities

WENXIA PAN[1], YE LI[1], KAI SUN[2], ZHU ZHU[1,3], AND XINRUI LI[1]

[1]College of Energy and Electrical Engineering, Hohai University, Nanjing 211100, China
[2]Huai'an Power Supply Branch, State Grid Jiangsu Electric Power Company, Huai'an 223003, China
[3]College of Electrical Engineering, Tongling University, Tongling 244000, China

Corresponding author: Ye Li (liyehhu.com@hhu.edu.cn)

This work was supported in part by the National Natural Science Foundation of China under Grant 51377047, in part by the 111 Project of Renewable Energy and Smart Grid under Grant B14022, and in part by the State Key Laboratory of Smart Grid Protection and Control under Grant SGNR0000KJJS1907536.

ABSTRACT The early fault of a cable is usually a incipient fault, which is difficult to find and can easily develop into an insulation breakdown fault. Thus, it is of great significance to quickly and accurately find an incipient cable fault. This paper presents an fault location method for cable insulation based on the electric quantities of both ends. Based on the equivalent circuit model of three-phase single-core cable distribution parameters, the calculation method of the voltage along the cable is derived. The equivalent model of cable insulation in resistive and capacitive parallel is proposed and applied to the early fault modeling of cable. On the basis of the calculation formula of the voltage along the cable and the electric quantity at both ends of the cable, the analytical expression of the cable fault location is obtained by solving the fault equation directly. Extensive simulations show that the algorithm, this method can locate the incipient fault accurately, and is not affected by the fault point, fault resistance and fault inception angle.

INDEX TERMS Cable insulation, fault location, distributed parameters, equivalent model, sheath current.

I. INTRODUCTION

Cables are widely used because they seldom require maintenance and are not affected by unfavorable climatic conditions. However, cable faults occur frequently in the processes of designing, manufacturing and constructing cables, and they are difficult to directly detect because most cables are buried directly underground or laid on the seabed [1]. Therefore, the rapid and accurate location of cable faults is of great significance to ensure the safe and stable operation of power systems [2], [3].

The cable material under different external factors can lead to aging factors that mainly include electric cable material aging, mechanical aging, thermal aging, environmental water aging (acid erosion, pollution, air flow, sand erosion, salt, etc.) and overload aging; aging is the direct result of material insulation performance degradation, which results in a decline in the reliability of the cable.

Cable faults can be divided into the main insulation fault, sheath fault, body fault and joint fault, depending on the fault location [4]. Since the main insulation of the cable is directly connected to the cable core, a main insulation fault will directly lead to a cable line or even a regional power outage. Therefore, this paper focuses on main insolation faults. If the cable is exposed to moisture for a long time, water branches will be generated in the insulation [5]. When the cable suffers lightning or over-voltage, the instantaneous over-voltage is enough to cause the water branch to be converted into an electric branch, leading to the cable insulation breaking down in a relatively short amount of time, resulting in a power outage [6], [7]. Before an insulation breakdown occurs in the cable, the occurrence of a power outage can be effectively reduced by finding the weak point of the insulation.

The early fault duration of the cable is short, so the overcurrent protection cannot be triggered, but the monitoring device can record the fault waveform. The existing cable fault location methods mainly include the traveling wave method, the impedance-based method, and the fault analysis method [8]. The traveling wave method [9]–[12] is not affected by the fault type, transition resistance, etc., and can be mainly divided into two types. One is to use the time difference between the transient traveling wave head to locate the fault, but it is difficult to detect the wave head and it is greatly affected by the fault angle [9], [10]. The other is to

The associate editor coordinating the review of this manuscript and approving it for publication was Behnam Mohammadi-Ivatloo.

make use of high voltage signals to induce partial discharge of the cables to perform traveling wave ranging [11], [12]. This method requires additional high voltage equipment. Therefore, it can only be detected off-line. The impedance-based method [2], [13], [14] simplifies the cable into a lump parameter model without considering the existence of a distributed capacitance, so the calculation error cannot be eliminated theoretically, and it cannot be applied when the fault resistance is large. The fault analysis method [15]–[17] uses the voltage, current and other electric quantities of the monitoring point after the fault occurs, and is combined with various characteristic parameters related to the system to establish the locating equation. After the analysis and calculation, the distance between the fault point and the monitoring point is solved. According to the different sources of the fault, the analysis can be divided into the single-end method and the both-ends method. The former [15], [16] method uses the voltage and current measured by a single end of the fault line to eliminate the unknown variables and obtain the fault distance by solving the locating equation. However, due to the lack of information, the single-end method has a principle defect. Boundary conditions usually need to be supplemented, but the solution to the equation becomes complicated, and the iterative search may cause the equation to not converge. The latter method [17] uses the electric quantities of both ends of the cable to form the location equation, which has sufficient, known information, and thus makes up for the deficiency in the single-end method, in principle.

In this paper, for a multiconductor system composed of a three-phase cable, the cable distribution parameter equivalent model [18], [19] is used to derive the calculation formulas of the voltage and current along the cable. For early cable failure caused by cable insulation aging, considering the influence of the metal sheath, the equivalent model of cable insulation in parallel with resistance and capacity is proposed and applied to the early fault modeling of cable. Considering the calculation formula of the voltage along the cable, based on the electric quantity at both ends of the cable and combined with the equivalent circuit model of a three-phase cable, the analytical expression of the cable fault location is obtained by directly solving the fault equation and diagonalizing the impedance matrix and admittance matrix by using the method of phase-mode transformation. A large number of simulation experiments were used to analyze the location of cables under different fault conditions, and the results show that this method can effectively locate the fault position.

II. THREE-PHASE CABLES TRANSMISSION MODEL

A. SINGLE-CORE CABLE STRUCTURE

The research object of this paper is a high voltage single-core Cross Linked Polyethylene (XLPE) cable, which is mainly composed of a conductor (core), semiconductive main insulation, a metal sheath, and outer insulation [20]. Its structure is shown in Fig. 1.

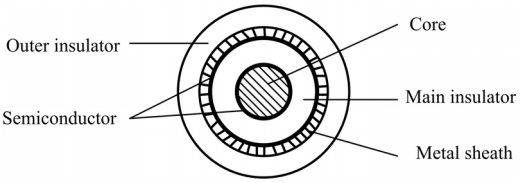

FIGURE 1. Structure of a single-core cable.

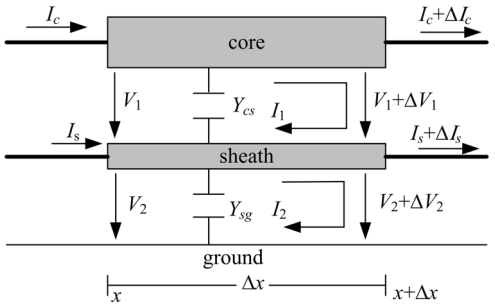

FIGURE 2. Distributed parameters model of single-core cable.

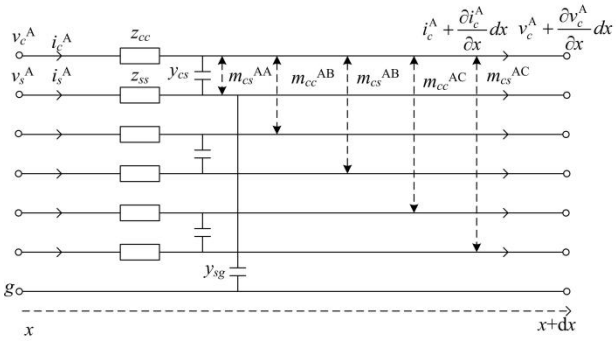

FIGURE 3. Distributed parameters cable model.

According to the single-core cable structure shown in Figure 1, the equivalent circuit model of single-core cable distribution parameters is shown in Figure 2. Loop 1 is composed of a wire core and a metal sheath, while loop 2 is composed of a metal sheath and earth. The mutual impedance between cable core and sheath is mainly caused by the fact that loops 1 and 2 share a metal sheath.

B. EQUIVALENT CIRCUIT MODEL

The cable sheath is regarded as a conductor that is parallel to the core, and the equivalent circuit model of the distributed parameters is established as shown in Fig. 3, including the three-phase core and the metal sheath of phases A, B and C.

There are six parallel conductors in total. Since the cables of each phase are compact coaxial cylinders and take the earth as the return circuit, the current in the A phase - earth circuit inevitably impacts the pressure drop in the B phase and C phase loops, which is reflected in the mutual impedance between phases. Here, z_{cc} is the impedance per unit length of the core, z_{ss} is the impedance per unit length of the sheath, and m is the mutual impedance per unit length. y_{cs} is the admittance per unit length between the core and the metal

sheath, while y_{sg} is the admittance per unit length between the sheath and the earth. g denotes ground, superscripts A, B and C represent the three phases, respectively, subscript c denotes the core, and subscript s denotes the metal sheath.

C. DERIVATION OF THE VOLTAGE FORMULA

As shown in Fig. 3 and taking phase A as an example, according to Kirchhoff's voltage law, the voltage expression can be obtained as follows:

$$\begin{aligned} V_c^{\mathrm{A}} &= V_c^{\mathrm{A}} + \frac{\partial V_c^{\mathrm{A}}}{\partial x}dx + z_{cc}dx \cdot I_c^{\mathrm{A}} + m_{cc}^{\mathrm{AB}}dx \cdot I_c^{\mathrm{B}} \\ &\quad + m_{cc}^{\mathrm{AC}}dx \cdot I_c^{\mathrm{C}} + m_{cs}^{\mathrm{AA}}dx \cdot I_s^{\mathrm{A}} + m_{cs}^{\mathrm{AB}}dx \cdot I_s^{\mathrm{B}} \\ &\quad + m_{cs}^{\mathrm{AC}}dx \cdot I_s^{\mathrm{C}} \end{aligned} \tag{1}$$

$$\begin{aligned} V_s^{\mathrm{A}} &= V_s^{\mathrm{A}} + \frac{\partial V_s^{\mathrm{A}}}{\partial x}dx + m_{cs}^{\mathrm{AA}}dx \cdot I_c^{\mathrm{A}} + m_{cs}^{\mathrm{AB}}dx \cdot I_c^{\mathrm{B}} \\ &\quad + m_{cs}^{\mathrm{AC}}dx \cdot I_c^{\mathrm{C}} + z_{ss}dx \cdot I_s^{\mathrm{A}} + m_{ss}^{\mathrm{AB}}dx \cdot I_s^{\mathrm{B}} \\ &\quad + m_{ss}^{\mathrm{AC}}dx \cdot I_s^{\mathrm{C}} \end{aligned} \tag{2}$$

The resolution of equations (1) and (2) has the following solution:

$$\begin{aligned} \frac{\partial V_c^{\mathrm{A}}}{\partial x} &= z_{cc} \cdot I_c^{\mathrm{A}} + m_{cc}^{\mathrm{AB}} \cdot I_c^{\mathrm{B}} + m_{cc}^{\mathrm{AC}} \cdot I_c^{\mathrm{C}} \\ &\quad + m_{cs}^{\mathrm{AA}} \cdot I_s^{\mathrm{A}} + m_{cs}^{\mathrm{AB}} \cdot I_s^{\mathrm{B}} + m_{cs}^{\mathrm{AC}} \cdot I_s^{\mathrm{C}} \end{aligned} \tag{3}$$

$$\begin{aligned} \frac{\partial V_s^{\mathrm{A}}}{\partial x} &= m_{cs}^{\mathrm{AA}} \cdot I_c^{\mathrm{A}} + m_{cs}^{\mathrm{AB}} \cdot I_c^{\mathrm{B}} + m_{cs}^{\mathrm{AC}} \cdot I_c^{\mathrm{C}} \\ &\quad + z_{ss} \cdot I_s^{\mathrm{A}} + m_{ss}^{\mathrm{AB}} \cdot I_s^{\mathrm{B}} + m_{ss}^{\mathrm{AC}} \cdot I_s^{\mathrm{C}} \end{aligned} \tag{4}$$

Similar to phase A, the voltage equations of phase B and phase C can be obtained. Therefore, the three-phase voltage formula can be expressed in the following matrix form,

$$-\frac{\partial}{\partial x}\begin{bmatrix} V_c \\ V_s \end{bmatrix} = \begin{bmatrix} Z_{cc} & Z_{cs} \\ Z_{cs} & Z_{ss} \end{bmatrix} \cdot \begin{bmatrix} I_c \\ I_s \end{bmatrix} \tag{5}$$

V_c, V_s and I_c, I_s represent the vectors of the voltages and currents related to the core and sheath conductors, respectively, which transposed are given by Eqs. (6), (7), (8) and (9),

$$V_c = [\, V_c^A \quad V_c^B \quad V_c^C \,]^T \tag{6}$$

$$V_s = [\, V_s^A \quad V_s^B \quad V_s^C \,]^T \tag{7}$$

$$I_c = [\, I_c^A \quad I_c^B \quad I_c^C \,]^T \tag{8}$$

$$I_s = [\, I_s^A \quad I_s^B \quad I_s^C \,]^T \tag{9}$$

The impedances matrices Z_{cc}, Z_{ss} and Z_{cs} are symmetrical and square of order 3 in the form:

$$Z_{cc} = \begin{bmatrix} z_{cc} & m_{cc}^{\mathrm{AB}} & m_{cc}^{\mathrm{AC}} \\ m_{cc}^{\mathrm{BA}} & z_{cc} & m_{cc}^{\mathrm{BC}} \\ m_{cc}^{\mathrm{CA}} & m_{cc}^{\mathrm{CB}} & z_{cc} \end{bmatrix} \tag{10}$$

$$Z_{ss} = \begin{bmatrix} z_{ss} & m_{ss}^{\mathrm{AB}} & m_{ss}^{\mathrm{AC}} \\ m_{ss}^{\mathrm{BA}} & z_{ss} & m_{ss}^{\mathrm{BC}} \\ m_{ss}^{\mathrm{CA}} & m_{ss}^{\mathrm{CB}} & z_{ss} \end{bmatrix} \tag{11}$$

$$Z_{cs} = \begin{bmatrix} m_{cs}^{\mathrm{AA}} & m_{cs}^{\mathrm{AB}} & m_{cs}^{\mathrm{AC}} \\ m_{cs}^{\mathrm{BA}} & m_{cs}^{\mathrm{BB}} & m_{cs}^{\mathrm{BC}} \\ m_{cs}^{\mathrm{CA}} & m_{cs}^{\mathrm{CB}} & m_{cs}^{\mathrm{CC}} \end{bmatrix} \tag{12}$$

In matrix Z_{cc}, in the diagonal are the self-impedances per unit length of the phase conductors and in the off diagonal are the mutual impedances per unit length between phases;

In matrix Z_{ss}, in the diagonal are the self-impedances per unit length of the sheaths and in the off diagonal are the mutual impedances per unit length between the sheaths;

In matrix Z_{cs}, in the diagonal are the mutual impedances per unit length between the core and sheath of the same phase and in the off diagonal are the mutual impedances per unit length between the core and sheath of different phases.

D. DERIVATION OF THE CURRENT FORMULA

Similar to the previous section, taking phase A as an example and according to Kirchhoff's current law, the following expression can be obtained.

$$I_c^{\mathrm{A}} = I_c^{\mathrm{A}} + \frac{\partial I_c^{\mathrm{A}}}{\partial x}dx + y_{cs}dx \cdot (V_c^{\mathrm{A}} - V_s^{\mathrm{A}}) \tag{13}$$

$$I_s^{\mathrm{A}} = I_s^{\mathrm{A}} + \frac{\partial I_s^{\mathrm{A}}}{\partial x}dx + y_{cs}dx \cdot (V_s^{\mathrm{A}} - V_c^{\mathrm{A}}) + y_{sg}dx \cdot V_s^{\mathrm{A}} \tag{14}$$

The resolution of the Eqs. (13) and (14) has the following solution:

$$-\frac{\partial I_c^{\mathrm{A}}}{\partial x} = y_{cs} \cdot V_c^{\mathrm{A}} - y_{cs}V_s^{\mathrm{A}} \tag{15}$$

$$-\frac{\partial I_s^{\mathrm{A}}}{\partial x} = -y_{cs} \cdot V_c^{\mathrm{A}} + (y_{cs} + y_{sg}) \cdot V_s^{\mathrm{A}} \tag{16}$$

Similar to phase A, the current equations of phase B and phase C can be obtained. Therefore, the three-phase current formula can be expressed in the following matrix form,

$$-\frac{\partial}{\partial x}\begin{bmatrix} I_c \\ I_s \end{bmatrix} = \begin{bmatrix} Y_{cc} & -Y_{cc} \\ -Y_{cc} & Y_{cc} + Y_{ss} \end{bmatrix} \cdot \begin{bmatrix} V_c \\ V_s \end{bmatrix} \tag{17}$$

The admittance matrices Y_{cc} and Y_{ss} are symmetrical and square of order 3 in the form:

$$Y_{cc} = \begin{bmatrix} y_{cs} & 0 & 0 \\ 0 & y_{cs} & 0 \\ 0 & 0 & y_{cs} \end{bmatrix} \tag{18}$$

$$Y_{ss} = \begin{bmatrix} y_{sg} & 0 & 0 \\ 0 & y_{sg} & 0 \\ 0 & 0 & y_{sg} \end{bmatrix} \tag{19}$$

In matrix Y_{cc}, y_{cs} is the core/sheath admittances per unit length of the phase conductors;

In matrix Y_{ss}, y_{sg} is the sheath/ground admittances per unit length of the metal sheath.

Through the above process, the matrix expressions of the three-phase cable voltage and current as shown in Eqs. (5) and (17) are obtained. The above voltage and current equations are abbreviated as:

$$\begin{aligned} -\frac{\partial V_j}{\partial x} &= Z_j I_j \\ -\frac{\partial I_j}{\partial x} &= Y_j Z_j \end{aligned} \tag{20}$$

where V_j and I_j, given by Eq. (19), respectively represent the voltages and currents vector of the cores and sheath. Z_j and Y_j, given by Eq. (22), respectively indicate the impedances and the admittances matrix of the same sequence.

$$V_j = [\, V_c^T \quad V_s^T \,]^T; \quad I_j = [\, I_c^T \quad I_s^T \,]^T \tag{21}$$

$$Z_j = \begin{bmatrix} Z_{cc} & Z_{cs} \\ Z_{cs} & Z_{ss} \end{bmatrix}; \quad Y_j = \begin{bmatrix} Y_{cc} & -Y_{cc} \\ -Y_{cc} & Y_{cc} + Y_{ss} \end{bmatrix} \tag{22}$$

E. DECOUPLING METHOD

By establishing the equivalent model of the three-phase cable, the voltage and current equations shown in Eq. (18) are derived, and the analytical formula for the cable terminal voltage and current can be obtained by solving this equation. However, the voltage and the current components in the equation are decoupled for the convenience of solution.

The voltage and the current equations in Eq. (18) are differentiated again, and the order 2 differential equations of the voltage and current are obtained, as shown in Eq. (21).

$$\begin{aligned} \frac{\partial^2 V_j}{\partial x^2} &= Z_j Y_j V_j \\ \frac{\partial^2 I_j}{\partial x^2} &= Y_j Z_j I_j \end{aligned} \tag{23}$$

It can be seen from Eq. (12) that the order 2 differential equation regarding voltage contains only a voltage variable, while the current equation contains only a current variable; that is, the decoupling between voltage and current is realized.

Both the impedance parameter matrix Z_j and the admittance parameter matrix Y_j are off-diagonal matrices, which reflect the existence of electromagnetic coupling with phases. The products Z_jY_j and Y_jZ_j between them are also nondiagonal matrices. Therefore, it is necessary to decouple Eq. (21) by means of a phase-mode transformation.

The essence of the phase-mode transformation is the similarity diagonalization of the matrix. The phase-mode transformation matrix is applied to the parameter product matrix Z_jY_j and Y_jZ_j to make it diagonalized. When the cable is not transposable, its impedance matrix and admittance matrix are both symmetric matrices, instead of the balance matrix. Therefore, in this case the fixed modulus transformation matrix used for a similarity transformation of the balance matrix cannot be adopted, and the selection of each element of the transformation matrix is related to the cable parameters.

The impedance matrix Z_j and admittance matrix Y_j are shown as follows:

$$Z_j = \begin{bmatrix} z_{cc} & m_{cs} & m_{cc}^{AB} & m_{cs}^{AB} & m_{cc}^{AC} & m_{cs}^{AC} \\ m_{cs} & Z_{ss} & m_{cs}^{AB} & m_{ss}^{AB} & m_{cs}^{AC} & m_{ss}^{AC} \\ m_{cc}^{AB} & m_{cs}^{AB} & Z_{cc} & m_{cs} & m_{cc}^{BC} & m_{cs}^{BC} \\ m_{cs}^{AB} & m_{ss}^{AB} & m_{cs} & Z_{ss} & m_{cs}^{BC} & m_{ss}^{BC} \\ m_{cc}^{AC} & m_{cs}^{AC} & m_{cc}^{BC} & m_{cs}^{BC} & Z_{cc} & m_{cs} \\ m_{cs}^{AC} & m_{ss}^{AC} & m_{cs}^{BC} & m_{ss}^{BC} & m_{cs} & z_{ss} \end{bmatrix} \tag{24}$$

$$Y_j = \begin{bmatrix} y_{cs} & -y_{cs} & 0 & 0 & 0 & 0 \\ -y_{cs} & y_{cs} + y_{cg} & 0 & 0 & 0 & 0 \\ 0 & 0 & y_{cs} & -y_{cs} & 0 & 0 \\ 0 & 0 & -y_{cs} & y_{cs} + y_{cg} & 0 & 0 \\ 0 & 0 & 0 & 0 & y_{cs} & -y_{cs} \\ 0 & 0 & 0 & 0 & -y_{cs} & y_{cs} + y_{cg} \end{bmatrix} \tag{25}$$

Regardless of the arrangement mode of the three-phase cable, there are:

$$\begin{aligned} m_{cc}^{AB} &= m_{cs}^{AB} = m_{ss}^{AB} \\ m_{cc}^{BC} &= m_{cs}^{BC} = m_{ss}^{BC} \\ m_{cc}^{AC} &= m_{cs}^{AC} = m_{ss}^{AC} \end{aligned} \tag{26}$$

Let $N = Y_jZ_j$. With N products of the matrix diagonalization algorithm for the parameters, obtain the corresponding eigenvalue and eigenvector T_i and $T_u = T_i^{-\mathrm{T}}$. T_i and T_u represent a phase transformation process, i.e., the current and voltage, respectively, as well as the decoupled model transformation matrix. The T_i and T_u mode transformation of the matrix function to the admittance matrix Y_j, the current column I_j and impedance matrix Z_j is shown in Eq. (27).

$$\begin{aligned} V_m(0) = T_u^{-1} V_j \quad I_m(0) = T_i^{-1} I_j \\ Z_m = T_u^{-1} Z_j T_i \quad Y_m = T_i^{-1} Y_j T_u \end{aligned} \tag{27}$$

By substituting Eq. (27) into Eq. (21), the order 2 differential equation of the voltage and current expressed by the modulus as shown in Eq. (28) can be obtained.

$$\begin{aligned} \frac{\partial^2 V_m}{\partial x^2} &= Z_m Y_m V_m \\ \frac{\partial^2 I_m}{\partial x^2} &= Y_m Z_m I_m \end{aligned} \tag{28}$$

where

$$V_m = [\, V_{mc}^A \quad V_{ms}^A \quad V_{mc}^B \quad V_{ms}^B \quad V_{mc}^C \quad V_{ms}^C \,]^T \tag{29}$$

$$I_m = [\, I_{mc}^A \quad I_{ms}^A \quad I_{mc}^B \quad I_{ms}^B \quad I_{mc}^C \quad I_{ms}^C \,]^T \tag{30}$$

III. ANALYTIC CALCULATION FORMULA FOR THE FAULT LOCATION

A. CALCULATION FORMULA FOR VOLTAGE

The original equation is obtained by a phase-mode transformation, where Z_m, Y_m and their products are diagonal matrices of order 6, $Z_mY_m = Y_mZ_m = \Lambda$, and Λ represents diagonal matrices.

$$\begin{aligned} \gamma &= \sqrt{Z_m \cdot Y_m} = \sqrt{Y_m \cdot Z_m} \\ Z_0 &= \sqrt{Z_m / Y_m} \end{aligned}$$

1) Take the electric quantities of the start-end of the cable as the known quantities.

Give the start-end voltage $V_m(0)$, current $I_m(0)$, and solve Eq. (28),

$$V_m(x) = \frac{e^{-\gamma x} + e^{\gamma x}}{2} V_m(0) - Z_0 \frac{e^{\gamma x} - e^{-\gamma x}}{2} I_m(0) \tag{31}$$

2) Take the electric quantities of the terminal of the cable as the known quantities.

Let the cable length be l, given the terminal voltage $V_m(l)$, current $I_m(l)$. Similar to 1), the difference lies in the solution to Eq. (28). The equation is an order 2 linear homogeneous differential equation with constant coefficients, and the general solution is as follows:

$$V_m(x) = c_1 e^{\gamma x} + c_2 e^{-\gamma x} \tag{32}$$

The initial conditions are as follows,

$$\begin{aligned} V_m(l) &= c_1 e^{\gamma l} + c_2 e^{-\gamma l} \\ V'_m(l) &= -Z_m I_m(l) = c_1 \gamma e^{\gamma l} - c_2 \gamma e^{-\gamma l} \end{aligned} \tag{33}$$

By solving Eq. (33),

$$\begin{aligned} c_1 &= \frac{\gamma \cdot V_m(l) - Z_m I_m(l)}{2\gamma \cdot e^{\gamma l}} \\ c_2 &= \frac{\gamma \cdot Vm(l) + Z_m I_m(l)}{2\gamma \cdot e^{-\gamma l}} \end{aligned} \tag{34}$$

By substituting Eq. (34) into Eq. (32),

$$V_m(x) = \frac{e^{-\gamma(x-l)} + e^{\gamma(x-l)}}{2} V_m(l) - Z_0 \frac{e^{\gamma(x-l)} - e^{-\gamma(x-l)}}{2} I_m(l) \tag{35}$$

Eqs. (31) and (35) are written as hyperbolic functions as follows:

$$V_m(x) = V_m(0) \cdot \cosh(\gamma x) - Z_0 I_m(0) \cdot \sinh(\gamma x) \tag{36}$$

$$V_m(x) = V_m(l) \cosh \gamma(x-l) - Z_0 I_m(l) \sinh \gamma(x-l) \tag{37}$$

Based on the above analysis process, the transmission equations of the three-phase single-core cable is derived, and the voltage calculation formula for the cable is solved. The voltage of the cable can be easily calculated by using Eqs. (36) or (37).

B. ANALYTICAL FORMULA FOR THE LOCATION

When a main insulation fault occurs at a certain point of the cable, the electrical quantity of the cable sheath will change significantly. Eqs. (36) and (37) respectively contain the electric quantities at the start-end and the terminal-end of the cable. Combining Eqs. (36) and (37), the analytical calculation method of the cable fault location x is deduced.

It can be seen from the forms of Eqs (36) and (37) that the reference points of calculation are both the start ends of the cable. Therefore, x in the two equations is consistent and represents the same point. Let Eq. (36) be equal to Eq. (37); then, the following formula for the cable fault location is obtained,

$$x = \frac{1}{\gamma} ar \tanh \frac{V_m(l)\cosh(\gamma l) + Z_0 I_m(l)\sinh(\gamma l) - V_m(0)}{V_m(l)\sinh(\gamma l) + Z_0 I_m(l)\cosh(\gamma l) - Z_0 I_m(0)} \tag{38}$$

Eq. (38) refers to the calculation method of the fault location by using the electrical quantities at both ends of the cable when taking the metal sheath into account.

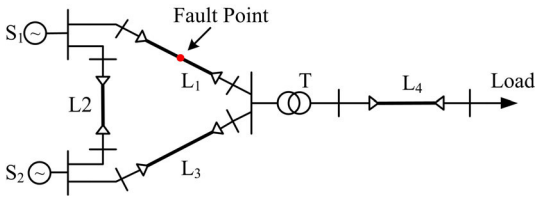

FIGURE 4. Schematic diagram of the 220 kV cables network system.

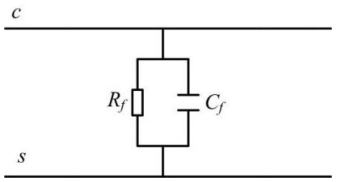

FIGURE 5. Equivalent circuit of the cable insulation.

IV. SIMULATION VERIFICATION

A. SIMULATION MODEL

This section focuses on the location of the main insulation in the case of a centralized fault in the cable network. A three-phase single-core cable network simulation model is built in PSCAD, and the cable main insulation fault is taken as an example to perform the simulation test.

As shown in Fig. 4, S_1 and S_2 are 220 kV and ideal power supplies with a phase difference of 1.05°. In the simulation model, the cable is equivalent to a four-layer structure with two semiconductive layers added (as shown in Fig.1). The radius of the core is 0.242 m, the main insulation radius is 0.05355 m, the radius of the metal sheath is 0.6085 m, the radius of the external insulation is 0.06875 m, and the thickness of the semiconductive layer is 0.001 m. Here, L1 is 40 km, L2 is 2 km, L3 is 40 km and L4 is 30 km. The transformer capacity is 180 MVA, the transformer ratio is 220/36.75 kV, and the percentage of short-circuit voltage is 10%.

The main insulation fault is simulated by a parallel circuit of the resistor and capacitor, as shown in Fig. 5, where R_f is the equivalent fault resistor and C_f is the equivalent fault capacitor. The relevant regulations stipulate that the $\tan\delta$ value be in the range of 0.0002∼0.0025 and the safety value be 0.008 when an XLPE cable is well insulated. The value of $\tan\delta$ is calculated by the following formula,

$$\tan\delta = \frac{1}{2\pi f R_f C_f} \tag{39}$$

where f is the frequency of the system.

The cable parameters are shown in Table 1.

B. INFLUENCE OF THE FAULT DISTANCE

Taking the insulation fault of the phase-A cable as an example, $R_f = 1\ \text{M}\Omega$, $C_f = 1\ \mu\text{F}$, $\tan\delta = 0.00318$, and core current is 0.3 kA. The voltage of the core terminal-end is shown in Fig. 6.

TABLE 1. Cable section and material parameters.

Parameters	Value
Distance between center and core/mm	24.2
Distance between center and inner insulator/mm	53.55
Distance between center and metal sheath/mm	60.85
Distance between center and outer insulator/mm	68.75
Core resistivity/Ω·m	1.72×10^{-8}
Metal sheath resistivity/Ω·m	2.2×10^{-7}
Permeability for core, metal sheath	1
Permittivity for inner insulator	2.5
Permittivity for outer insulator	2.3

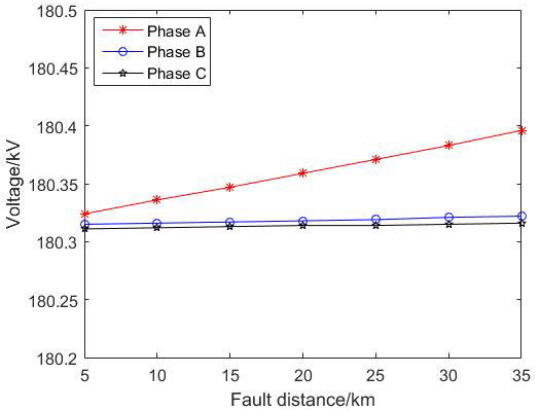

FIGURE 6. The voltage at the end of the cable core.

According to the comparison of the results in Fig. 6, with an increase in the fault distance, the voltage of the fault phase (Phase A) core has a small increase, but the increase amplitude is not more than 0.02%, and the voltage of the nonfault phase has no change. At this point, the cable can supply power normally.

As both ends of the metal sheath are grounded, an induced voltage is generated in the metal sheath, resulting in an induced current. When the fault distance changes, the sheath current will change accordingly. The sheath current of different fault distances is shown in Fig. 7.

It can be seen from Fig. 7 that the sheath current of the fault phase decreases with an increase in the fault distance, while the sheath current of the nonfault phase almost remains the same with an increase in the fault distance.

Based on the results in Fig. 6 and Fig. 7, the existence of an early fault in the case of sheath grounding can be judged by the characteristics of no significant change in the fault phase voltage and a significantly increased fault phase sheath current. By substituting the voltage and current values of both ends of the cable into Eq. (38), the fault location of the cable can be obtained through calculation. In the actual cable fault, the site maintenance personnel should find the fault point in time and eliminate the hidden trouble. Therefore, absolute error is selected to represent the location accuracy in this paper.

$$\varepsilon = |d_e - d_a| \tag{40}$$

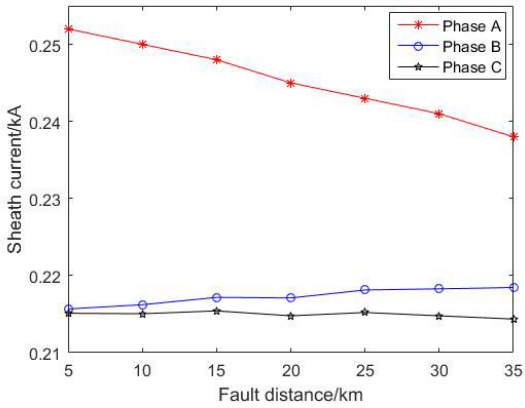

FIGURE 7. The sheath current at the head of the cable.

TABLE 2. Result of the fault location.

d_a (km)	d_e (km)	ε (km)
5	5.054	0.054
10	10.068	0.068
15	15.091	0.091
20	20.106	0.106
25	25.103	0.103
30	30.113	0.113
35	35.124	0.124

where ε represents the absolute error of the fault location, d_e is the calculated fault distance, and d_a is the actual fault distance. The location results are shown in Table 2.

According to the results in Table 2, the method deduced from this paper has a high location accuracy at different fault points, with the maximum error not exceeding 0.124 km.

C. INFLUENCE OF THE FAULT SEVERITY

According to the analysis in the previous section, when a cable insulation fault occurs, it will have an impact on the electrical quantities of the cable. Considering the influence of different fault severities on the location accuracy, both ends of the sheath are grounded. The core current is 0.3 kA, the core voltage of the terminal-end is shown in Fig. 8, and the sheath current of the start-end is shown in Fig. 9. The fault severities are as follows:

(a). $R_f = 0.5$ MΩ, $C_f = 1$ μF, $\tan\delta = 0.00637$;
(b). $R_f = 0.05$ MΩ, $C_f = 1.05$ μF, $\tan\delta = 0.0606$.

As seen from Fig. 8, with an increase in the fault distance, the voltage of fault phase increases slightly. When the main insulation fault of the cable is further deepened, the voltage of the fault phase at the same fault point does not change significantly.

It can be seen from Fig. 9 that at the same fault point, with a deepening of the insulation fault, the sheath current did not change significantly because the dielectric loss caused by the early-stage concentrated insulation fault of the cable is only a small part, so it had little impact on the overall sheath current value. Therefore, under a different severity of the fault, there

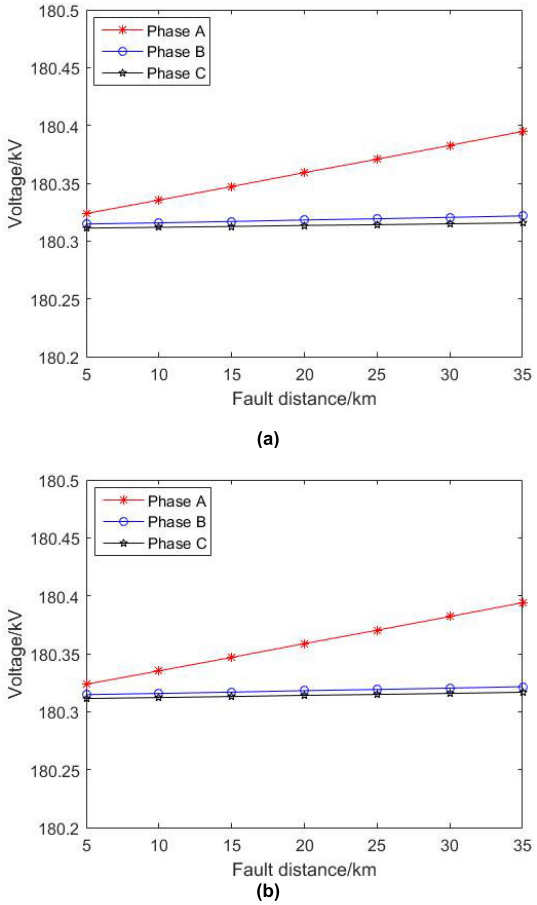

FIGURE 8. The voltage at the end of the cable core. (a).$R_f = 0.5$ MΩ, $C_f = 1$ μF, (b).$R_f = 0.05$ MΩ, $C_f = 1.05$ μF.

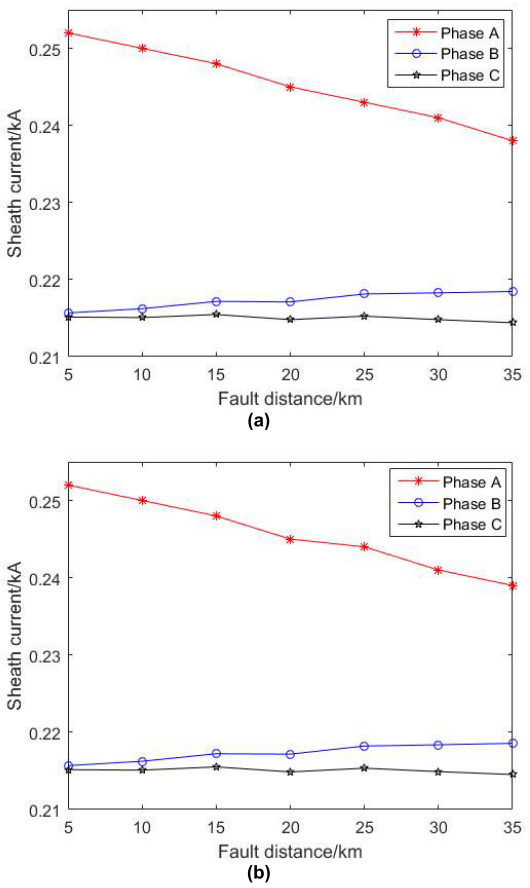

FIGURE 9. The sheath current at the head of the cable. (a).$R_f = 0.5$ MΩ, $C_f = 1$ μF, (b).$R_f = 0.05$ MΩ, $C_f = 1.05$ μF.

TABLE 3. Fault location results with different fault severities.

d_a (km)	Fault severity	d_e (km)	ε (km)
5	a	5.047	0.047
	b	5.049	0.049
10	a	10.069	0069
	b	10.064	0.064
15	a	15.088	0.088
	b	15.080	0.080
20	a	20.097	0.097
	b	20.091	0.091
25	a	25.113	0.113
	b	25.105	0.105
30	a	30.098	0.098
	b	30.095	0.095
35	a	35.102	0.102
	b	35.119	0.119

is no obvious difference in the electric quantities, such as the sheath current and terminal-end voltage at the same fault point. The ratio of the fault phase sheath current to the core current is greater than 0.795.

The location results are shown in Table 3.

According to the results of Table 3, the proposed method has a high location accuracy for different fault severities, with the maximum error not exceeding 0.119 km.

D. INFLUENCE OF THE GROUNDING MODE

Let $R_f = 0.1$ MΩ, $C_f = 1$ μF and $\tan\delta = 0.0318$. The core current is 0.3 kA. With the fault distance in different grounding modes, Fig. 10 show the variation in the core voltage at the terminal-end and Fig. 11 show the variation of the sheath current at the start-end.

It can be seen from Fig. 10 and Fig. 11 that under the two grounding modes, the voltage of the fault phase has no significant change, and under different fault distances, the maximum change in fault voltage does not exceed 0.042%. In the case of single-end grounding, the change in the nonfault phase sheath current is more obvious than that in the case of both-ends grounding. With an increase in the fault distance, the ratio of the nonfault phase sheath current to the core current in the case of single-end grounding is 0.814. The location results are shown in Table 4.

As seen from Table 4, the method presented in this paper is well applicable to the main insulation fault location of a cable when the metal sheath is grounded by the single-end and both-ends method. The maximum errors under the two grounding modes are not more than 0.117 km.

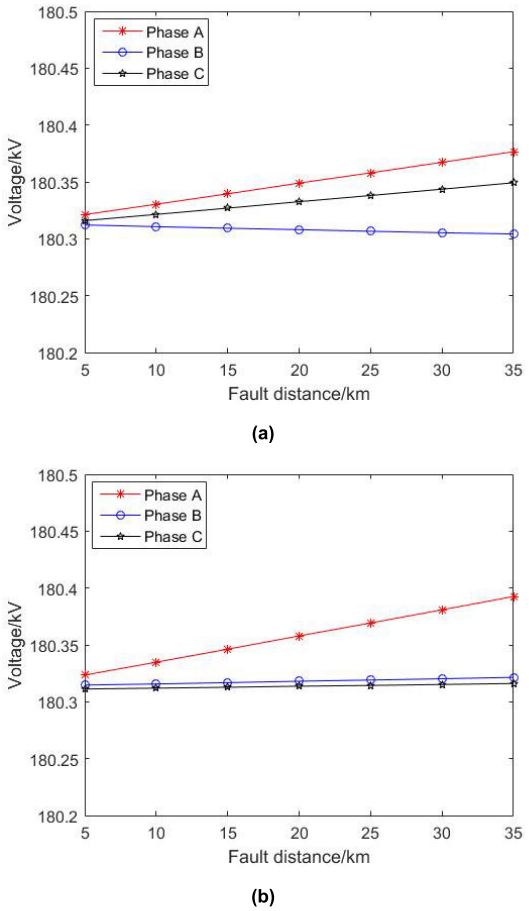

FIGURE 10. The voltage at the end of the cable core. (a) Single-end grounding, (b) both-ends grounding.

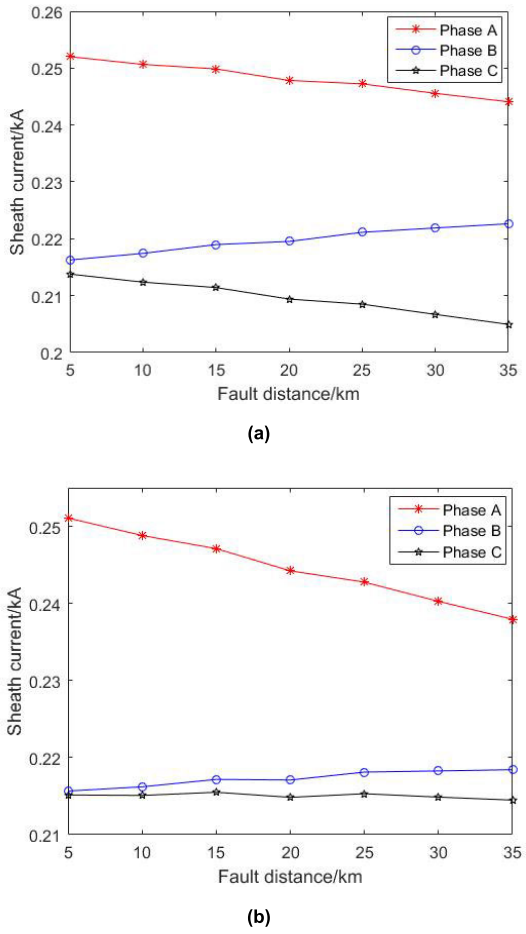

FIGURE 11. The sheath current at the head of the cable. (a) Single-end grounding, (b) both-ends grounding.

TABLE 4. Results with different sheath grounding methods.

d_a (km)	Fault scenarios	d_e (km)	ε (km)
5	a	5.038	0.038
	b	5.044	0.044
10	a	10.053	0.053
	b	10.062	0.062
15	a	15.073	0.073
	b	15.082	0.082
20	a	20.083	0.083
	b	20.094	0.094
25	a	25.088	0.088
	b	25.104	0.104
30	a	30.089	0.089
	b	30.096	0.096
35	a	35.106	0.106
	b	35.117	0.117

E. CROSS BONDING

This section discusses the problem of fault location under the cross bonding of the metal sheath. The fault type adopts the same main insulation fault as in the previous sections. The core current is 0.3 kA, $R_f = 0.05$ MΩ, $C_f = 1.05$ μF, and $\tan\delta = 0.0606$. The cable parameters are the same as in Table 1, and the cable length is 4.5 km. The metal sheath is connected by means of cross bonding, which usually divides an entire cable into several large segments and divides each segment of three small segments. The schematic diagram of the cable cross bonding is shown in Fig. 12.

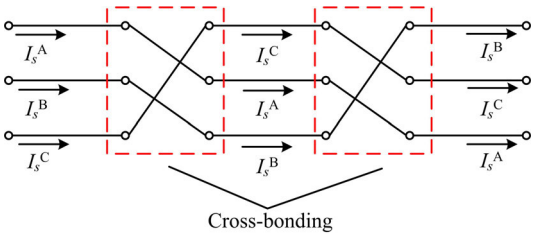

FIGURE 12. Schematic diagram of the cross-bonding of the metal sheath.

The simulation model is built in PSCAD, and the schematic diagram is shown in Fig. 13. The simulation results show that in the case of cross bonding, the ratio of the fault phase sheath current to the core current is 0.214, and the fault phase sheath current to the nonfault phase sheath current is 13.26. The results of the fault location are shown in Table 5.

As shown in Table 5, in the case of cross bonding, the error of the location results do not exceed 0.041 km, indicating that the fault location method described in this paper is suitable for the case of cross bonding of a metal sheath.

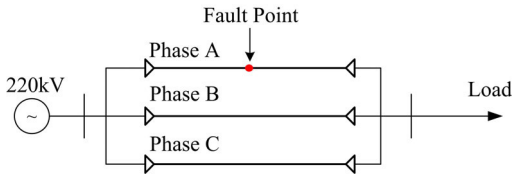

FIGURE 13. Schematic diagram of a simulation model for a 220 kV three-phase single-core cable.

TABLE 5. Location results with sheath cross-bonding.

d_a (km)	d_e (km)	ε (km)
0.5	0.460	0.040
1.0	1.026	0.026
1.5	1.541	0.041
2.0	2.029	0.029
2.5	2.537	0.037
3.0	3.025	0.025
3.5	3.523	0.023
4.0	4.041	0.041

TABLE 6. Distance error with different fault inception angles.

fault inception angle(°)	d_e (km)	ε (km)
0	1.981	0.019
30	2.027	0.027
60	2.054	0.054
90	2.079	0.079

TABLE 7. Distance error with different fault resistances.

fault resistance(MΩ)	d_e (km)	ε (km)
0.02	1.958	0.042
0.04	1.966	0.034
0.06	2.013	0.013
0.08	2.043	0.043
0.5	1.964	0.036
1.0	1.891	0.109
1.1	1.882	0.118
1.2	1.878	0.122
1.5	1.866	0.134

F. INFLUENCE OF FAULT INCEPTION ANGLE(1, 5)

The core current is 0.3 kA, $R_f = 0.05$ MΩ, $C_f = 1.05$ μF, the fault distance is 2 km and the fault inception angle is 0°, 30°, 60° and 90°. The fault location result is shown in Table 6.

According to the results in Table 6, the location error increases as the fault inception angle increases.

G. INFLUENCE OF FAULT RESISTANCE

The core current is 0.3 kA, $C_f = 1.05$ μF, the fault distance is 2 km, the fault inception angle is 0°, and the fault resistance is 0.02 MΩ to 1.5 MΩ. The fault location result is shown in Table 7.

As shown in Table 7, the location accuracy increases with a decrease in fault resistance. This is because as the aging degree of the cable deepens, the fault resistance of the decreases, the current flowing through the metal sheath also increases, and the location result is more accurate.

TABLE 8. Distance error with different loads.

load(MW)	d_e (km)	ε (km)
10	1.948	0.052
20	1.968	0.032
40	1.946	0.054
60	1.973	0.027
80	1.981	0.019
100	1.995	0.005

TABLE 9. Distance error with different solution time steps.

step(μs)	d_e (km)	ε (km)
0.2	1.981	0.019
0.4	1.981	0.019
0.6	1.981	0.019
0.8	1.981	0.019
1.0	1.981	0.019

H. INFLUENCE OF LOAD

The fault distance is set as 2 km, the fault inception angle is 0°, $R_f = 0.05$ m, $C_f = 1.05$ μF, and the load is set as 10 MW to 100 MW. The fault location result is shown in Table 8.

According to the results shown in Table 8, the overall trend of the location accuracy is that it improves as the load increases.

I. INFLUENCE OF THE SOLUTION TIME STEP

The core current is 0.3 kA, $R_f = 0.05$ MΩ, $C_f = 1.05$ μF, the fault distance is 2 km, the fault inception angle is 0°, and the simulation step is set from 0.2 μs to 1.0 μs. The fault location result is shown in Table 9.

According to the location results in Table 9, the simulation step size has no influence on the location accuracy.

V. CONCLUSION

Based on the basic structure of a single-core XLPE cable and the cable double π equivalent circuit model, this paper deduced the calculation formula for the voltage along a cable based on the both-ends electric quantities of the cable, and used the phase-mode transformation to decouple the formula. On this basis, a fault location method suitable for single-end and both-ends grounding of the sheath is proposed.

In this paper, we considered main insulation incipient fault cases, set different fault severities and different grounding modes, and obtained the fault distance through calculations. The results show that this method has a better location accuracy, the maximum error under non cross-bonding does not exceed 0.124 km, and the maximum error under cross-bonding does not exceed 0.134 km.

REFERENCES

[1] F. Dinmohammadi, D. Flynn, C. Bailey, M. Pecht, C. Yin, P. Rajaguru, and V. Robu, "Predicting damage and life expectancy of subsea power cables in offshore renewable energy applications," *IEEE Access*, vol. 7, pp. 54658–54669, 2019.

[2] S. Zhang, S. Lin, J. Tang, and Z. Y. He, "Fault location of self-clearing fault in three phase single core cables based on double impedance model," *Trans. China Electrotech. Soc.*, vol. 31, no. 17, pp. 1–10, Sep. 2016.

[3] M. Marzinotto and G. Mazzanti, "The feasibility of cable sheath fault detection by monitoring sheath-to-ground currents at the ends of cross-bonding sections," *IEEE Trans. Ind. Appl.*, vol. 51, no. 6, pp. 5376–5384, Nov. 2015.

[4] *IEEE Guide for Fault-Locating Techniques on Shielded Power Cable Systems*, Standard 1234-2007, Mar. 2019.
[5] L. J. Zhou, Q. P. Qiu, R. Cheng, Y. Chen, D. C. Liu, and L. L. Zhang, "Influence of partial air pressure on propagation and partial discharge characteristics of electrical trees in XLPE cable under different temperatures," *Proc. CSEE*, vol. 36, no. 18, pp. 5094–5103, Sep. 2016.
[6] B. Sheng, W. Zhou, J. Yu, S. Meng, C. Zhou, and D. M. Hepburn, "On-line PD detection and localization in cross-bonded HV cable systems," *IEEE Trans. Dielectr. Electr. Insul.*, vol. 21, no. 5, pp. 2217–2224, Oct. 2014.
[7] T. S. Sidhu and Z. Xu, "Detection of incipient faults in distribution underground cables," *IEEE Trans. Power Del.*, vol. 25, no. 3, pp. 1363–1371, Jul. 2010.
[8] *IEEE Guide for Determining Fault Location on AC Transmission and Distribution Lines*, Standard C37.114-2014, Dec. 2014.
[9] Y. Liu, Y. Shi, J. Guo, and Y. Wang, "Application of pulse compression technique in fault detection and localization of leaky coaxial cable," *IEEE Access*, vol. 6, pp. 66709–66714, Nov. 2018.
[10] R. Liang, Z. Jin, and C. L. Wang, "Research of fault location in distribution networks based on integration of travelling wave time and frequency analysis," *Proc. CSEE*, vol. 33, no. 28, pp. 130–136, Oct. 2013.
[11] M. Bawart, M. Marzinotto, and G. Mazzanti, "Diagnosis and location of faults in submarine power cables," *IEEE Elect. Insul. Mag.*, vol. 32, no. 4, pp. 24–37, Jul. 2016.
[12] M. Gilany, D. K. Ibrahim, and E. S. Tag Eldin, "Traveling-wave-based fault-location scheme for multiend-aged underground cable system," *IEEE Trans. Power Del.*, vol. 22, no. 1, pp. 82–89, Jan. 2007.
[13] S. Das, S. Santoso, A. Gaikwad, and M. Patel, "Impedance-based fault location in transmission networks: Theory and application," *IEEE Access*, vol. 2, pp. 537–557, 2014.
[14] Z. Xu and T. S. Sidhu, "Fault location method based on single-end measurements for underground cables," *IEEE Trans. Power Del.*, vol. 26, no. 4, pp. 2845–2854, Oct. 2011.
[15] X. Yang, M.-S. Choi, S.-J. Lee, C.-W. Ten, and S.-I. Lim, "Fault location for underground power cable using distributed parameter approach," *IEEE Trans. Power Syst.*, vol. 23, no. 4, pp. 1809–1816, Nov. 2008.
[16] J. Tang, S. Zhang, and S. Lin, "Single-terminal fault locating method of cables considering the metal sheath structure," *Proc. CSEE*, vol. 36, no. 6, pp. 1748–1756, Mar. 2016.
[17] M. Li, C. Zhou, and W. Zhou, "A revised model for calculating HV cable sheath current under short-circuit fault condition and its application for fault location—Part 1: The revised model," *IEEE Trans. Power Del.*, vol. 34, no. 4, pp. 1674–1683, Aug. 2019.
[18] T. Aloui, F. B. Amar, and H. H. Abdallah, "Modeling and simulation of a HV shielded underground three-phase cable in both normal and default states: Application to the 150 kV connection between Taparoura, Sidimansour and Tyna substations in Sfax-Tunisia," *Electr. Power Syst. Res.*, vol. 141, pp. 91–99, Dec. 2016.
[19] T. Aloui, F. B. Amar, and H. H. Abdallah, "Fault prelocalization of underground single-phase cables: Modeling and simulation," *Int. J. Electr. Power Energy Syst.*, vol. 44, no. 1, pp. 514–519, Jan. 2013.
[20] W. Liang, Z. Zhou, W. Pan, Y. Li, Q. Zhou, and M. Zhu, "Study on the calculation and suppression method of metal sheath circulating current of three-phase single-core cable," in *Proc. IEEE PES Asia–Pacific Power Energy Eng. Conf. (APPEEC)*, Dec. 2019, pp. 1–5.

WENXIA PAN received the B.S. and M.S. degrees from Wuhan University, Wuhan, China, in 1982 and 1987, respectively, and the Ph.D. degree from Hohai University, Nanjing, China, in 2004. She is currently a Professor of electrical engineering with Hohai University. She has published two research books and authored or coauthored over 100 journal articles. Her current research interests include renewable energy generation systems, and high-voltage and insulation technology.

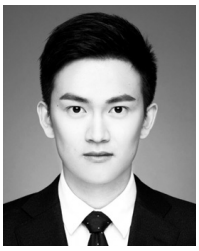

YE LI received the B.S. degree in electrical engineering, in 2018. He is currently pursuing the M.S. degree in electrical engineering with Hohai University, Nanjing, China. His main research interests include wind power generation technology, and high-voltage and insulation technology.

KAI SUN received the M.S. degree from Hohai University, Nanjing, China, in 2019. He is currently an Engineer with Huai'an Power Supply Branch, State Grid Jiangsu Electric Power Company, engaged in power grid operation and monitoring. His main research interests include high-voltage and insulation technology, especially power cable technology and power transmission technology.

ZHU ZHU received the M.S. degree in photovoltaic and renewable energy engineering from the University of New South Wales (UNSW), Sydney, NSW, Australia, in 2011. She is currently pursuing the Ph.D. degree in electrical engineering with Hohai University, Nanjing, China. Her main research interest includes renewable energy generation technology.

XINRUI LI received the B.S. degree in electrical engineering in 2016. She is currently pursuing the M.S. degree in electrical engineering with Hohai University, Nanjing, China. Her main research interests include wind power generation technology, and high-voltage and insulation technology.